Evolution of Pseudo-Spherical Silicon Nanocrystals to Tetrahedra, Mediated by Phosphonic Acid Surfactants

C A Barrett[1], Calum Dickinson[1], S. Ahmed[1], T Hantschel[2], K Arstila[2] and K M Ryan[1]

[1] Materials and Surface Science Institute and Department of Chemical and Environmental Sciences, University of Limerick, Limerick, Ireland
[2] Interuniversitair Micro-Elektronica Centrum, Kapeldreef 75 B-3001, Leuven, Belgium

E-mail: kevin.m.ryan@ul.ie

Abstract
Silicon nanocrystals were synthesised at high temperatures and high pressures by the thermolysis of diphenylsilane using a combination of supercritical carbon dioxide and phosphonic acid surfactants. Size and shape evolution from pseudo-spherical silicon nanocrystals to well faceted tetrahedral-shaped silicon crystals with edge lengths in the range of 30-400 nm were observed with sequentially decreasing surfactant chain lenghts. The silicon nanocrystals were characterized by transmission electron microscopy (TEM), energy-dispersive X-ray spectroscopy (EDX), X-ray diffraction (XRD), photoluminescence (PL), scanning electron microscopy (SEM) and Raman scattering spectroscopy.

1. Introduction

Silicon nanocrystals are promising candidate materials with prototypical device applications as flash memory,[1, 2] field configurable transistors[3] and third generation solar cells.[4] Consequently, facile routes to size controlled nanocrystalline silicon in useable quantities are widely sought. Free-standing silicon nanoparticles have been prepared using gas-phase and solution decomposition of silanes,[5, 6] solution-based precursor reduction[7, 8] and physical methods involving the use of plasma or pulverization and sonication of porous silicon.[9, 10] Size and shape control in the solution synthesis of silicon has not been significantly achieved in comparison to II-VI nanocrystals where an understanding of facet specific surfactant passivation during nucleation and growth allows size monodisperse nanocrystals of a range of geometric shapes to be routinely generated.[11] Alkyl phosphine or alkyl phosphinyl oxide surfactants are particularly effective as they dynamically adsorb on to the surface of the nanocrystal facilitating defined growth.[12] Solution phase reactions with trioctylphosphine (TOP) are widely used for II-VI nanocrystal growth as crystal nucleation occurs below 400°C, which is within the boiling point of the hot surfactant.[13] Group IV germanium nanocrystals, that can be nucleated at low temperatures by means of thermal reduction of a halide precursor, can be dynamically stabilized with TOP but this has not been extended to silicon due to the much higher temperatures (>500°C) required.[14] Surfactant passivated silicon tetrahedra with an edge length of ~200 nm were achieved using a two step synthesis by Baldwin et al.[15] This method involving low temperature silicon halide solution reductions followed by surface termination has been further used for the formation of sub 5 nm silicon nanocrystals by selective modification of the inorganic precursors.[16] The capping ligands in these cases act only to solubilize the nanocrystals in organic solvents and are not part of the nucleation and growth process. Warner et al. demonstrated a degree of size and shape control with a reverse micelle synthesis of germanium nanocrystals. By increasing the rate of precusor reduction, to raise monomer concentrations during nucleatation, an evolution from smaller (5 nm) spherical nanocrystals to larger (50 nm) triangular shaped nanocrystals was achieved.[17] Group IV nanocrystal synthesis in high temperature solvents has been achieved whereby a supercritical fluid acts as both a passivating medium and solvent.[18] Holmes et al.

synthesized pseudo-spherical silicon nanocrystals of 1.5 nm in diameter using supercritical octanol, although termination occurred quickly (< 3 nm), limiting the realization of size and shape control.[6] Supercritical carbon dioxide (sc-CO_2) is an attractive solvent for nanocrystal synthesis as it promises a cleaner alternative to conventional organics for bulk synthesis.[19] Lu et al. previously demonstrated that sc-CO_2 could be used as a solvent, in conjunction with octanol as a capping ligand for the formation of germanium nanocrystals.[20] Ryan et al. also utilized CO_2 for the growth of silicon nanowires in mesoporous films although non-templated or non-seeded silicon nanocrystal synthesis in CO_2 has not been reported to-date.[21] Here we report a modification of the supercrtical thermolysis route to nanocrystals, whereby using CO_2 and selected phosphonic acid surfactants, a size and shape modulation from pseduo-spherical to well faceted tetrahedral-shaped silicon nanocrystals was obtained.

2. Experimental details

2.1 Materials and Apparatus

All chemicals were used as received unless otherwise stated. Diphenylsilane (97%) and Trioctylphosphine (>90%) used was received from Sigma-Aldrich and stored and dispensed from a nitrogen filled glove box. Alkyl phosphonic acids: octadecylphosphonic acid (ODPA), dodecylphosphonic acid (DDPA) and hexylphophonic acid (HPA) were supplied from PolyCarbon Industries Inc. Experiments were conducted using Liquid Carbon Dioxide from BOC (99.85%) and the reaction cells, stainless steel tubing and connections were all supplied from High Pressure Equipment Co. The micro reactors used were of a grade-2 titanium construction, designed specifically for high temperatures and pressures. A Teledyne Model 260D Computer Controlled Syringe Pump was used to pressurize the system and an Applied Test Systems Inc. Model 3210, 3-zone heating furnace, was used to regulate temperature.

2.2 Synthesis and Purification

The silicon nanocrystals were synthesized by thermal decomposition of diphenylsilane (DPS) in the presence of trioctylphosphine (TOP) and an alkyl phosphonic acid, at 600°C and 35 MPa in supercritical CO_2. Alkyl phosphonic acid/TOP solutions were prepared by mixing 20 µl of a desired phosphonic acid with 80 µl (0.202 mmol) of TOP, giving a 1:4 volume ratio. The solutions were then degassed at 120°C and 100 mtorr for one hour, to remove any water present in solution, before being stored under an inert atmosphere. The reactions were carried out in a 5 ml high pressure titanium grade-2 reaction cell. In a typical experiment, a reaction cell was loaded with 100 µl of an alkyl phosphonic acid and TOP solution and 100 µl (0.523 mmol) of DPS under an inert atmosphere of a nitrogen filled glove box. The cell was sealed under nitrogen and then removed from the glovebox where it was then connected to the computer controlled syringe pump using ⅛ inch stainless steel high pressure tubing. Using the syringe pump, liquid CO_2 was pumped into the reaction cell and the pressure was increased above its critical point (T_c = 31°C, P_c = 7.1 MPa), to 28 MPa. The 3-zone heating furnace was preheated to 615°C, 15°C above the required reaction temperature of 600°C. The reactor was placed in the furnace and reached the desired temperature of 600°C in under a minute. When the system had stabilized at the desired temperature, the pressure was further increased to 35 MPa. Both temperature and pressure were then kept constant for the proceeding reaction time of 2 hours, at which point the furnace was opened and cooled to room temperature. CO_2 was then vented from the reaction cell leaving a black powder residue.

Chloroform was injected into the cell and subsequently removed to extract the nanocrystals from the reactor. All samples were initially centrifuged at 4000 rpm for 10 minutes to remove a precipitate, containing carbon byproducts of the reaction. The Si nanocrystals were then precipitated by adding 5-10 ml of acetone and centrifuging at 5000 rpm for 10 minutes. The remaining solution was discarded and the precipitate was re-dispersed with 5 ml of chloroform. These steps were repeated twice more before the precipitate was again re-dispersed in 10 ml of chloroform for analysis. All

samples were sealed in glass vials which were stored in a nitrogen filled glove box to prevent against nanocrystal oxidation.

2.3 Characterization

Crystal morphology and size distribution were evaluated by transmission electron microscopy (TEM) and selected area electron diffraction (SAED) using a JEOL JEM-2011 electron microscope operated at an accelerating voltage of 200 kV using a LaB_6 filament. The chemical composition analysis was performed using energy dispersive X-ray spectroscopy (EDX) with a Princeton Gamma Tech Prism 1G system with a 10 mm^2 silicon detector and an INCAPentaFET-x3, with a Si(Li) detector and a 30 mm^2 detecting crystal. X-ray diffractograms were recorded on a Philips X'Pert PRO MPD (multi-purpose x-ray diffractometer), using a Cu-K_α radiation source and standard scintillation detector. The scanning electron microscopy (SEM) images of the as-synthesized samples were obtained by a Hitachi S-4800 and a Philips XL-30 high resolution scanning electron microscope operated at 5 kV. Photoluminescence spectra were recorded with a Varian Cary Eclipse fluorescence spectrophotometer. Raman spectrums were recorded on a Dilor XY Labram spectrometer with detected Ar ion laser irradiation of $\lambda = 514$ nm.

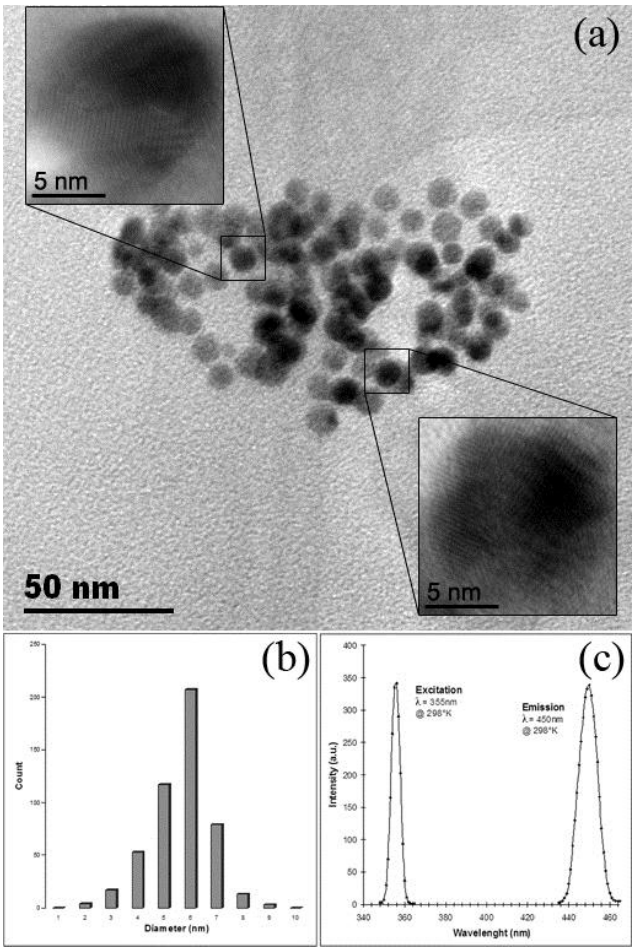

Fig. 1 (a) Low and high resolution TEM images of an area of silicon nanocrystals synthesised with ODPA and (b) the corresponding particle size distribution histogram. Room temperature photoluminescence spectrum with excitation at 335 nm and the corresponding emission peak at 450 nm (c).

3. Results and Discussion

Sequentially decreasing the carbon chain length of the alkyl phosphonic acid component, added to the reaction mixture (1:4:5 volume ratio with TOP and DPS respectively), influenced the size and shape of the silicon nanocrystals obtained. Figure 1(a) shows the TEM analysis of silicon nanocrystals, collected from reactions using ODPA as the capping ligand. HRTEM images (inset) of two individual nanoparticles, taken from an area of high concentration, show visible lattice fringes outlining their pseuodo spherical nanostructure. Several of the Si nanocrystals showed fringes with a lattice spacing of 0.192 nm, which matches well with the (220) plane of diamond cubic silicon. The mean diameter, calculated from a survey of particle sizes from several regions (Figure 1(b)), gave a value of 5.7 nm with a standard deviation of ±0.1 nm. In all reactions with the 18 carbon chain (C18) ODPA, there was no observation of tetrahedral-shaped nanocrystals. Given the mean size of the Si nanocrystals being close to that of the Bohr excitation radius for Si (r = 4.9 nm), no visible luminescence was observed, which is suggestive of a low confinement regime. Room temperature photoluminescence analysis was carried out on a diluted chloroform dispersion of as-prepared silicon nanocrystals collected from a synthesis using ODPA. The photoluminescence spectrum (Figure 1(c)), shows a relatively narrow region of intense luminescence with a maximum intensity centered at 450 nm, with an excitation at 355 nm. Silicon nanocrystals, ranging from 1 to 5 nm in diameter, have been shown to exhibit PL emission ranging from blue to the near-infrared.[22] In this case, reactions using ODPA seem to produce blue emitting silicon nanocrystals. Given that the photoluminescence could be affected by both the particle size and surface, it is assumed that oxidation of the nanocrystal surfaces is a contributing factor to the blue shift in emission. This has typically been observed for other silicon nanocrystal studies, where the nanocrystal surface had been oxide passivated.[23]

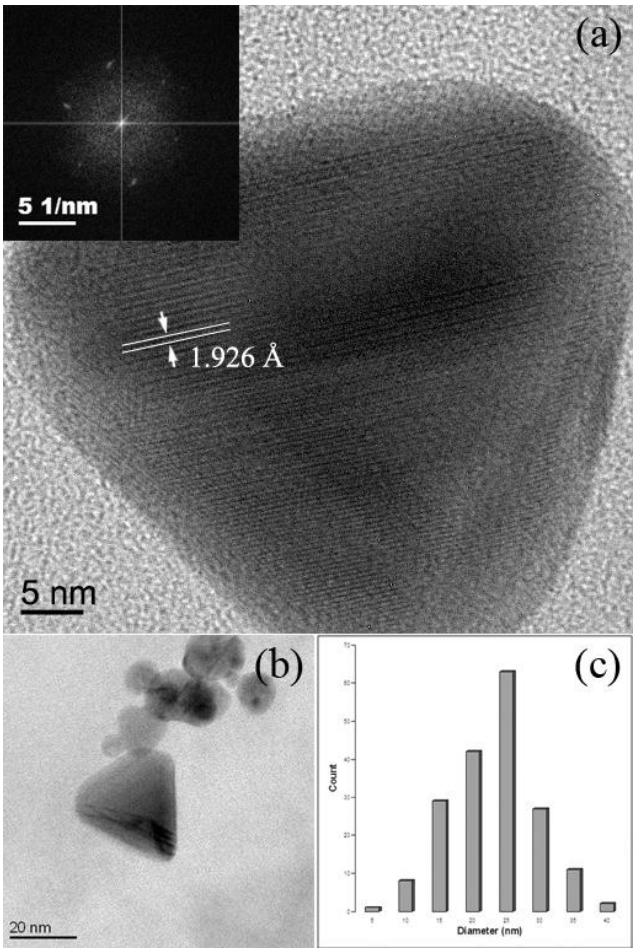

Fig. 2 HRTEM image of a truncated tetrahedral-shaped nanocrystal with corresponding fast Fourier transform inset (a). TEM image of a mixture of truncated nanotetrahedra and pseudo spherical nanocrystals synthesized using DDPA (b) with the corresponding particle size distribution histogram (c).

The synthesis with DDPA (C12) yielded a mixture of pseudo-spherical nanocrystals as well as truncated nanotetrahedra (Figure 2(a)). The particle size distribution range was found to be from 5 to 40 nm (Figure 2(b)). However for the tetrahedral-shaped nanocrystals alone, the edge length was measured at 15-40 nm, where as the spherical nanoparticles were found to have diameters ranging from 5 to 15 nm. A HRTEM image in Figure 2(c) displays a typical silicon nanotetrahedron truncated at each vertex, with an interplanar spacing of 0.192 nm. This is in good agreement with the d spacing of the (220) plane for diamond structural crystalline silicon. A fast Fourier transform (FFT) analysis, shown in the inset, gives a spot array of the 3D lattice fringes. The three-dimensional nature of the FFT, corresponds to the visible lattice fringing running parallel to the edges of the crystal facets.

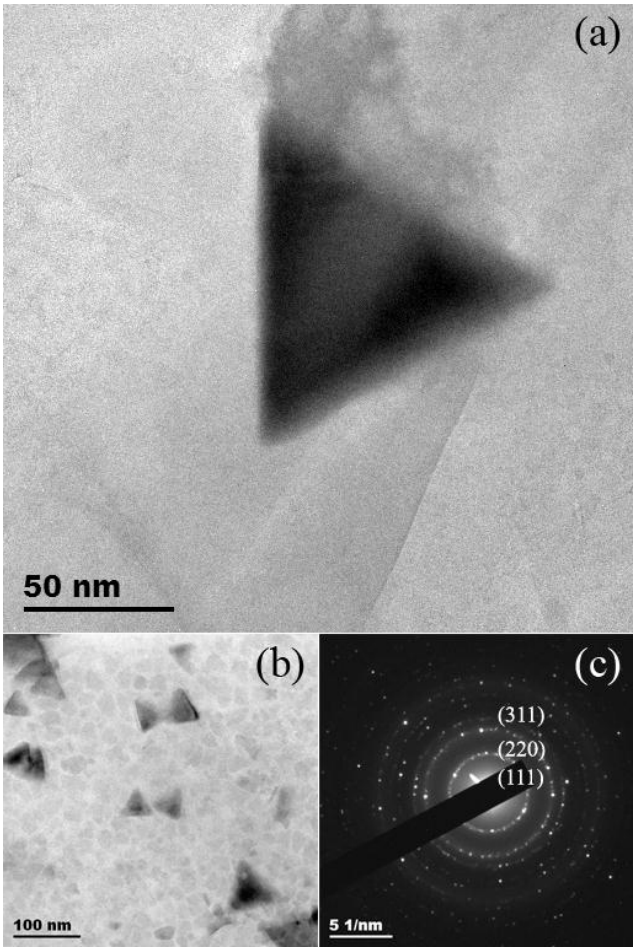

Fig. 3 High and low resolution TEM images of tetrahedral-shaped nanocrystals, synthesis using HPA (a,b) with the corresponding selective area electron diffraction pattern (c).

HPA (C6) reactions yielded high concentrations of tetrahedral-shaped silicon crystals (Figure 3(a)) which were found, on average, to have an edge length below 100 nm. There was no evidence of smaller particles, such as those observed in reactions using ODPA or DDPA, with the majority of the yield having a regular tetrahedral symmetry of four enclosing (111) facets. Observations of significant truncation was apparent for tetrahedra with edge lengths of less than 50 nm. Electron diffraction

analysis of several typical crystals from a synthesis using HPA (Figure 3(b)), gave a polycrystalline diffraction pattern, from which the maximum intensity of the diffraction rings gave d spacings of 0.312, 0.191, and 0.162 nm (Figure 3(c)). These spacings correspond to the lattice parameters of (111), (220) and (311) for diamond cubic crystalline silicon. It is known that different crystallographic planes usually have different surface energies.[24] In this case, the surface energy of the {111} plane is lower than those of the {100} and {110} planes. In the formation of the larger crystal structures (50-400 nm), a tetrahedron has the minimal surface energy, owing to the four {111} equivalent facets. However, for the smaller (15-40 nm), tetrahedral-shaped nanocrystals, the vertices contain much fewer atoms, with the force of attraction being weaker in these areas. Thus, the atoms at the vertices are not as tightly bound, and truncated tetrahedral nanocrystals are generated. Below this minium size (<15 nm), atom clusters seem to favour a pseuodo-spherical structure.

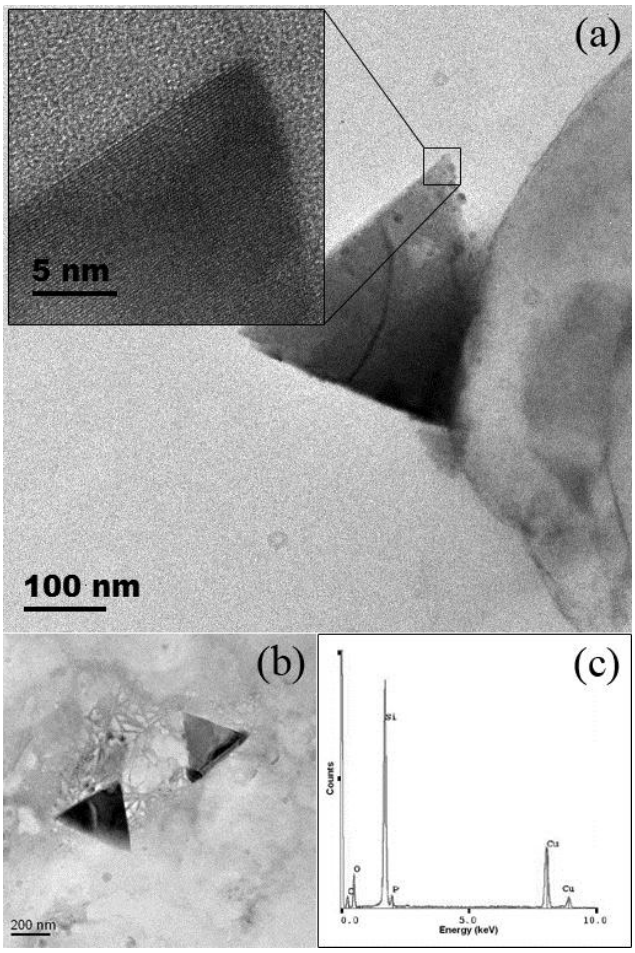

Fig. 4 TEM image (a) of a Si tetrahedron and the corresponding HRTEM image of one vertex inset. TEM image (b) of Si tetrahedra synthesis using only TOP, with the corresponding EDX spectrum (c).

It was found that when experiments were conducted in the complete absence of alkyl phosphonic acids, where only TOP and DPS was used, larger, fully formed silicon tetrahedral-shaped crystals were produced (Figure 4(a,b)). These crystals were found to be of the order of 200-400 nm in edge length. The HRTEM analysis (inset) of one vertex of a silicon tetrahedron, shows a highly crystalline structure with a measured interplanar spacing of 0.191 nm between the visible lattice fringes. EDX analysis of a selection of silicon tetrahedra synthesised with out the use of any alkyl phosphonic acid is shown in Figure 4(c). A strong Si peak is observed with lower intensity peaks of O, P, Cu, and C.

The copper and carbon peaks originated from the copper TEM grid and its amorphous carbon film support, while the minor oxygen and phosphorous peaks are expected due to the presence of residual TOP and its oxidised form TOPO, in the sample. The orientation of the tetrahedra with respect to the electron microscope beam (Figure 5(a-c)), shows how the tetrahedral morphology, when viewed as a 2D transmission image, results in a triangular shape with dimensions dependent on the orientation of the tetrahedral crystal with respect to the incident beam. The computer-aided design (CAD) images (inset) show the most likely 3D construction of the silicon nanocrystal corresponding to each image, with the assumption of a regular tetrahedral morphology. It is presumed that the tetrahedra in Figure 5(c) and 5(d) are not resting squarely on a facet, where as in Figure 5(c), the equal edge lengths and angular ratios, indicate that one side of the tetrahedron is perpendicular to the beam. The corresponding selected area electron diffraction of Figure 5(c), shown in Figure 5(d), indicates that the synthesised tetrahedra are pure single crystal silicon. The indexed Bragg reflections for this nanocrystal correspond to the [111] zone axis which is expected from a regular tetrahedron sitting on a (111) faceted base. Calculations for the hexagonal pattern give a spacing of 0.192 nm, which can be indexed for the (220) and (202) directions of diamond cubic silicon with interplanar angles of 60°. From this result, we can deduce that the basal plane of the crystal is (111).

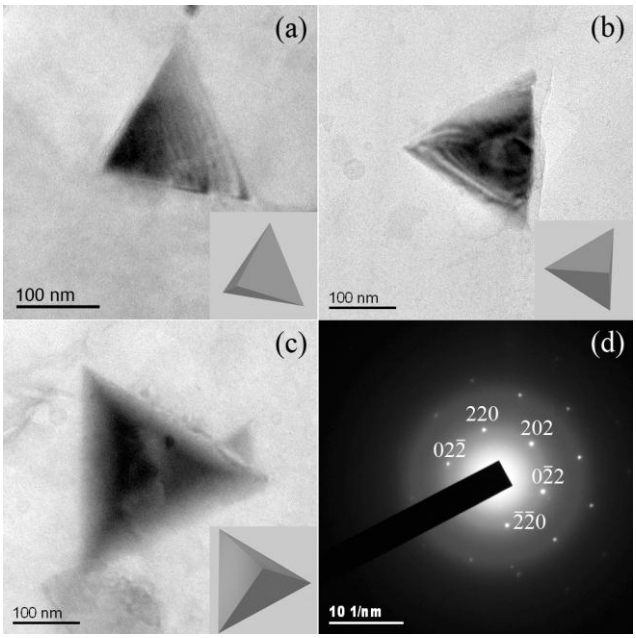

Fig. 5 TEM images of silicon tetrahedra with inset CAD models, portraying their geometrical orientation (a-c). A single crystal pattern (d), from the selective area electron diffraction analysis of (c).

Since TEM images display only the projection of the nanocrystals onto the observed plane, SEM measurements were taken to more accurately characterize the three dimensional tetrahedral structure. Figure 6(a) and 6(b) shows SEM images of silicon tetrahedra, synthesized from a typical TOP/DPS reaction and deposited on a conductive substrate, with typical edge lengths of approximately 350 nm. In Figure 6(a) the tetrahedron is sitting with one face parallel to the substrate giving a plan view of the other three (111) facets. It is known that tetrahedral-shaped nanocrystals have Td symmetry in which three triangular faces meet at each vertex. The nanocrystal is lying in a similar orientation to that portrayed in Figure 5(c), thus making it difficult to discern the apex of the tetrahedron. In contrast, the apex of the silicon tetrahedron is more clearly defined in Figure 5(b), however in this case the angle of alignment allows only two (111) facets to be resolved. From SEM it is clear that depending on the nanocrystal angle of alignment either one, two or three faces on a tetrahedron may be directly visible at any one time.[25] From the EDX spectrum displayed in Figure 6(d), a strong silicon signal is

apparent when focusing on the area shown in Figure 6(c), which is in good agreement with the EDX analysis carried out under TEM. The SEM analysis confirms that the nanocrystals obtained show a regular silicon tetrahedral morphology, with no evidence of truncation or platelet formation observed.

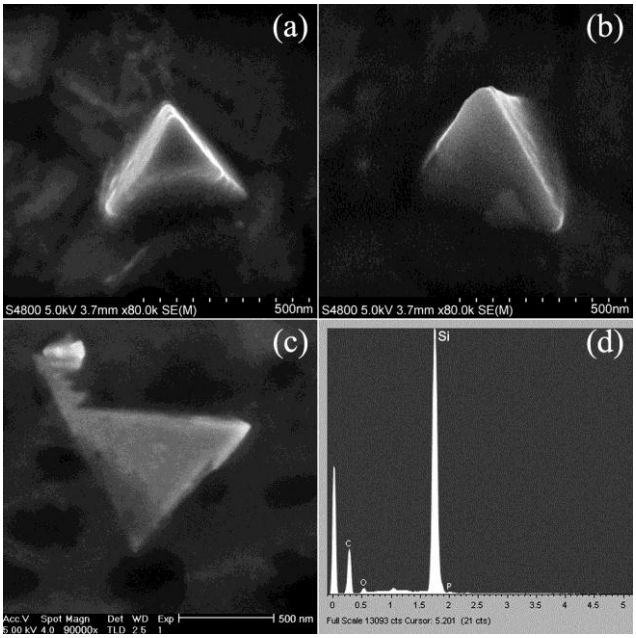

Fig. 6 HRSEM images (a,b) of well faceted silicon tetrahedra, synthesized from a TOP/sc-CO_2 system. SEM image (c) of silicon tetrahedra with corresponding EDX spectrum (d).

Figure 7(a) shows a typical powder X-ray diffraction pattern collected from 200 mg of powder containing tetrahedral-shaped silicon nanocrystals, retrieved from a typical synthesis using only TOP and DPS. Strong peak reflections were observed at $2\theta = 28.32°$, 47.25°, 56.13°, 69.08° and 76.61° respectively, consistent with the (111), (220), (311), (400) and (331) peaks for diamond lattice silicon. The positions and intensities of all broadened reflections agree with the selected area electron diffraction analysis obtained from nanocrystals of the same sample and are consistent with the diamond cubic morphology of crystalline silicon. A broad peak at approximately 24° in the pattern is consistent with observations of large micron sized spheres of amorphous silicon oxide, observed as a byproduct in the sample. This is consistent with observations from other previously reported methods of silicon nanoparticle production.[26, 27] XRD analysis from samples collected from control experiments, where TOP, DPS or CO_2 were omitted from a typical synthesis, found that no crystalline material was formed in their absence. Without the use of TOP in conjunction with the supercritical fluid, large lumps of amorphous silicon could be produced.

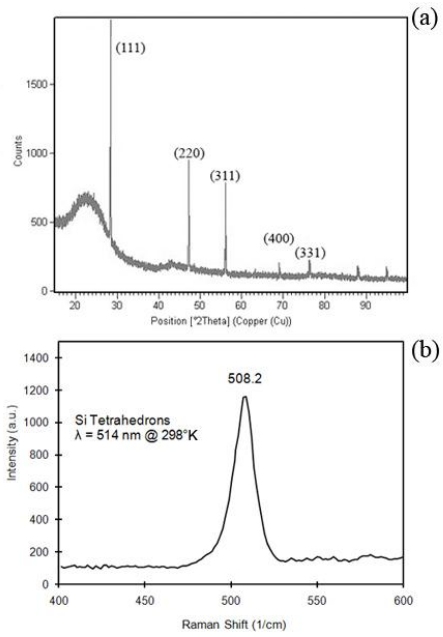

Fig. 7 An example of a XRD spectrum collected from as-synthesized black powders (a). The XRD pattern indexes to diamond cubic Si and also shows a broad peak at the beginning which can be attributed to silicon oxide by-products. Raman spectrum of TOP capped silicon tetrahedra (b).

The Raman spectrum, shown in Figure 7(b), was collected from the same sample of the silicon tetrahedra and deposited on an ethyl cellulose background. A strong peak at 508.2 cm^{-1} was observed for the 200-400 nm sized silicon tetrahedra which was not evident in the scans for the smaller sized nanocrystals where relatively weaker peak intensities were found centered around 519 cm^{-1}. The asymmetric peak at 508.2 cm^{-1} slightly broadens out towards 480 cm^{-1} which can be attributed to the presence of silicon oxide where Raman scattering between 450 and 500 cm^{-1} is typical. It is generally accepted that for bulk crystalline silicon, a peak position at 520 cm^{-1} can be found[28] however Raman spectra of Si nanowires have been recorded in literature at down-shifted peak positions of 515 to 500 cm^{-1} for wires of 10-30 nm in diameter.[29, 30] This Raman downshift has been attributed to the quantum size effect from nanocrystalline samples or heating of the samples by the laser during analysis. It is worth noting however that besides the optical phonon confinement effect, the effect of stress within silicon nanocrystals has also been reported to cause a down-shift in peak positions. Liu et al. suggested that the Raman shift seen for their larger sized silicon nanocubes (200-500 nm) was not due to the quantum size effect but instead attributed to the crystalline defects in the silicon cubes themselves.[31] Similarly, given the larger size of the silicon tetrahedra, we believe that the down-shifted peak can also be contributed to crystalline defects, such as dislocations which were routinely observed under TEM and SEM analysis.

It would seem apparent that phosphonic surfactants have a large degree of influence on silicon crystal growth in this synthesis and demonstrate good stability at high reaction temperatures (600°C) and elevated pressures of the supercritical carbon dioxide. Clearly, the sequential addition of long chain hydrocarbons to the TOP/DPS solution has resulted in a gradual increase in particle size and has influenced crystal shape. The schematic shown in Figure 8, highlights the three dimensional morphological change which has occurred, where the only change in the reaction parameters for each synthesis is a reduction in the carbon chain length of the phosphonic acid surfactant component. It has been demonstrated that hydrocarbon ligands provide some degree of steric stabilization in the formation of nanocrystals in sc-CO_2.[32] The repulsive forces of the surface passivated nanoparticles are determined by the surface coverage of the capping ligands, the length of the ligand tail and the solvent quality.[19] In the context of this study, a poor solvent such as sc-CO_2 would cause the ligand

tails to collapse partially, augmenting the overall attractive forces and increasing the aggregation of nuclei during the reaction. As the nucleation of nanoparticles occurs from the decomposition of the silicon monomer, reactions using only TOP (a weakly coordinating solvent) would be expected to form large nanocrystals due to a higher amount of nuclei aggregation. The van der Waals attraction between nanocluster cores is screened by steric repulsion from the addition of phosphonic capping ligands on the nanocrystals. ODPA, with the longest alkyl tail, gave the smallest particles thus showing the greatest reduction in nuclei aggregation.

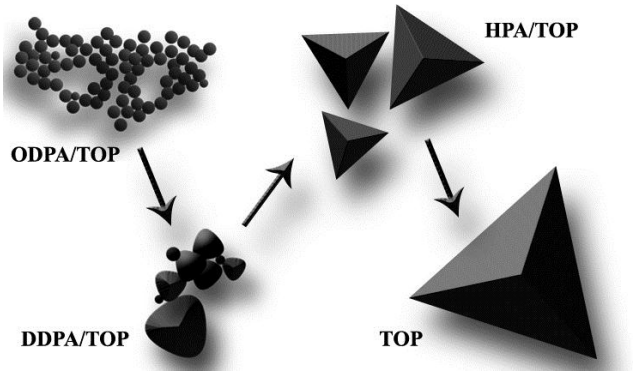

Fig. 8 A schematic showing the effect of the phosphonic acid on the size and shape evolution of pseudo spherical silicon nanocrystals to larger truncated nanotetrahedra and finally to fully formed silicon tetrahedral-shaped crystals.

The inclusion of the alkyl phosphonic acids, demonstrate an expected varied degree of screening with respect to the different ligand tail lengths. As a result a degree of control over the size and shape evolution, from pseudo-spherical silicon nanocrystals to well faceted tetrahedral-shaped silicon crystals, can be demonstrated. The thermodynamic growth observed is governed by the Gibbs-Curie-Wulff theorem, which suggests that the shape of a crystal is determined by the relative surface free energy of individual crystallographic faces.[33] The final crystal shape results from minimizing the total free energy of the system. In our case, silicon nanoclusters convert to the thermodynamically favored uniform tetrahedral nanoparticles by dissolution and regrowth of monomer. It is likely that the passivating influence of TOP helps silicon nanoclusters nucleate in the shape of rudimental tetrahedra.

4. Conclusions

In summary, by successfully utilizing TOP and alkyl phosphonic acids, as both coordinating and capping ligands, we have prepared well faceted tetrahedral-shaped silicon nanocrystals through utilisation of a supercritical CO_2 system. The shape of the nanocrystals evolves sequentially through nucleation and growth within the constraints of steric stabilisation afford by the particular alkyl phosphonic surfactant used. The presence of the alkyl phosphonic acids, demonstrate a degree of stabilisation for the initial nuclei and hindered any further regrowth, resulting in size control. Polyhedral shapes with well defined facets and corners have been shown to have distinct scattering signatures and scattering efficiencies.[24] Further development in surfactant mediated growth control of group (IV) nanocrystals may allow more complex anisotropic shaped structures such as nanorods, to be formed.

Acknowledgements

This work was supported by Science Foundation Ireland (SFI) through the Principal Investigator program, contract No. 06/IN.1/I85. The authors acknowledge Gordon Armstrong for assistance with Raman spectroscopy, which was facilitated by the Higher Education Authority's Program for

Research in Third Level Institutions. Noel Buckley is further acknowledged for access to Hitachi S4800 HRSEM.

[1] Thean A and Leburton J P 2001 *J. Appl. Phys.* **89** 2808
[2] Sandip T, Farhan R, Hussein H, Allan H, Emmanuel F C and Kevin C 1996 *Appl. Phys. Lett.* **68** 1377
[3] Lai Q, Li Z, Zhang L, Li X, Stickle W F, Zhu Z, Gu Z, Kamins T I, Williams R S and Chen Y 2008 *Nano Lett.* **8** 876
[4] Beard M C, Knutsen K P, Yu P, Luther J M, Song Q, Metzger W K, Ellingson R J and Nozik A J 2007 *Nano Lett.* **7** 2506
[5] P. Roca i Cabarrocas, T. Nguyen-Tran, Y. Djeridane, A. Abramov, Johnson E and Patriarche G 2007 *J. Phys. D: Appl. Phys.* **40** 2258
[6] Holmes J D, Ziegler K J, Doty R C, Pell L E, Johnston K P and Korgel B A 2001 *J. Am. Chem. Soc.* **123** 3743
[7] Pettigrew K A, Liu Q, Power P P and Kauzlarich S M 2003 *Chem. Mater.* **15** 4005
[8] Heath J R 1992 *Science* **258** 1131
[9] Neiner D, Chiu H W and Kauzlarich S M 2006 *J. Am. Chem. Soc.* **128** 11016
[10] Bapat A, Gatti M, Ding Y-P, Campbell S A and Kortshagen U 2007 *J. Phys. D: Appl. Phys.* **40** 2247
[11] Manna L, Scher E C and Alivisatos A P 2000 *J. Am. Chem. Soc.* **122** 12700
[12] Alivisatos A P 1996 *J. Phys. Chem.* **100** 13226
[13] Yin Y and Alivisatos A P 2005 *Nature* **437** 664
[14] Lu X M, Korgel B A and Johnston K P 2005 *Chem. Mater.* **17** 6479
[15] Baldwin R K, Pettigrew K A, Garno J C, Power P P, Liu G Y and Kauzlarich S M 2002 *J. Am. Chem. Soc.* **124** 1150
[16] Baldwin R K, Pettigrew K A, Ratai E, Augustine M P and Kauzlarich S M 2002 *Chem. Commun.* 1822
[17] Warner J H and Tilley R D 2006 *Nanotechnology* **17** 3745
[18] Shah P S, Hanrath T, Johnston K P and Korgel B A 2004 *J. Phys. Chem. B* **108** 9574
[19] Lu X M, Korgel B A and Johnston K P 2005 *Nanotechnology* **16** S389
[20] Lu X M, Ziegler K J, Ghezelbash A, Johnston K P and Korgel B A 2004 *Nano Lett.* **4** 969
[21] Ryan K M, Erts D, Olin H, Morris M A and Holmes J D 2003 *J. Am. Chem. Soc.* **125** 6284
[22] Hua F, Erogbogbo F, Swihart M T and Ruckenstein E 2006 *Langmuir* **22** 4363
[23] Lin S-W and Chen D-H 2009 *Small* **5** 72
[24] Tao A, Prasert S and Yang P D 2006 *Angew. Chem., Int. Ed.* **118** 4713
[25] Ng C H B and Fan W Y 2007 *J. Phys. Chem. C* **111** 9166
[26] Liu S, Sato S and Kimura K 2005 *Langmuir* **21** 6324
[27] Hessel C M, Henderson E J and Veinot J G C 2006 *Chem. Mater.* **18** 6139
[28] Li B, Yu D and Zhang S-L 1999 *Phys. Rev. B* **59** 1645
[29] Shu-Lin Z, Wei D, Yan Y, Jiang Q, Bibo L, Le-yu L, Kwok To Y and Dapeng Y 2002 *Appl. Phys. Lett.* **81** 4446
[30] Chen Y, Peng B and Wang B 2007 *J. Phys. Chem. C* **111** 5855
[31] Liu P, Cao Y L, Cui H, Chen X Y and Yang G W 2008 *Chem. Mater.* **20** 494
[32] Shah P S, Husain S, Johnston K P and Korgel B A 2001 *J. Phys. Chem. B* **105** 9433
[33] Mullin J W 1997 *Crystallization* (Oxford: Butterworth-Heinemann)